JOURNAL OF SYNCHROTRON RADIATION
ISSN 1600-5775

Geometric determination of direction of dislocations using synchrotron X-ray transmission topography

T. O. Tuomi,[a]* A. Lankinen[a,b] and O. Anttila[a,c]

[a]Department of Electronics and Nanoengineering, Aalto University, PO Box 13500, FIN-00076 Aalto, Finland, [b]Okmetic Oy, Piitie 2, FI-01510 Vantaa, Koivuhaka, Finland, and [c]Finsil Ltd, Saunamaentie 11, 02770 Espoo, Finland. *Correspondence e-mail: turkka.o.tuomi@aalto.fi

Received 16 December 2019
Accepted 17 August 2020

Edited by A. Bergamaschi, Paul Scherrer Institut, Switzerland

Keywords: X-ray topography; X-ray diffraction.

When performing transmission polychromatic beam topography, the extensions to the line segments of the diffraction images of a straight dislocation are shown to intersect at a single point on the X-ray film. The location of this point, together with the diffraction pattern recorded on the film by synchrotron radiation, gives the crystallographic direction [*hkl*] of the dislocation unambiguously. The results of two synchrotron topography experiments are presented. Very long dislocations found in the center of a large 450 mm-diameter Czochralski silicon crystal align with the growth direction [001]. In the other silicon sample, the dislocations are of mixed type and along the [01$\bar{1}$] direction.

1. Introduction

Figure 1 shows a usual experimental setup for recording X-ray topographs in a synchrotron radiation laboratory. The high-intensity, incident X-ray beam of a bending-magnet source has a continuous spectrum of radiation. The highly parallel rays hit a plate-like monocrystalline sample, where diffraction occurs at multiple wavelengths (Tuomi *et al.*, 1973; Tuomi, 2002). The diffracted beams form a Laue pattern (Friedrich *et al.*, 1913) of diffraction images on a high-resolution X-ray film, which is put behind or in front of the sample, perpendicular to the incident beam. Each diffraction image, *i.e.* a topograph, reveals microscopic features of dislocations, as well as those of other defects, which may be present in the sample. In this paper, we consider dislocations in such a setup, in which the film is located behind the sample, and the method is then called transmission topography, as opposed to back-reflection topography.

The dislocations usually appear as dark (*i.e.* large X-ray intensity) lines with a width of about 5 µm in the diffraction topographs, if the diffraction phenomenon corresponds to the low-absorption case; whereas in the case of *anomalous transmission* the lines are white, *i.e.* lack of X-ray intensity (Authier, 2001). In both cases a dislocation is characterized by two vectors: (i) the vector $\vec{\ell}$ parallel to the dislocation line and (ii) the vector $\vec{b}$, which is called the Burgers vector.

The vector $\vec{\ell}$ identifies the crystallographic direction of the dislocation line, which is the primary topic of this paper. Most of the topographs on the film reveal the dislocations when present. The direction of a dislocation appears to vary from one topograph to another. These images can be used to define the three-dimensional crystallographic direction of the defect. Some topographs, however, may be such that the image contrast disappears fully, or almost completely. The Burgers

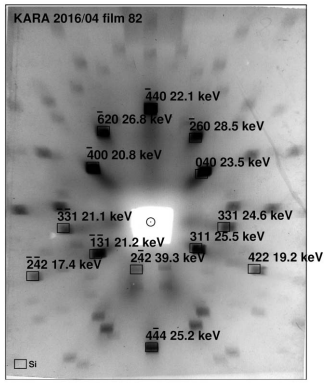

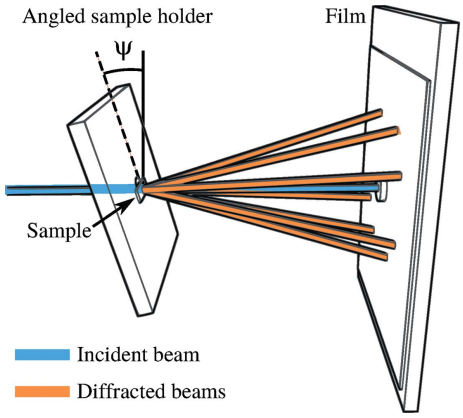

Figure 1
Schematic of the transmission topography geometry. The film is perpendicular to the beam, whereas the sample holder is tilted at an angle Ψ.

vector $\vec{b}$ of a dislocation can be identified if its image contrast is found to disappear in two or more topographs, the Miller indices of which are known.

A technique called *stereo topography* has been used for visualizing dislocations in three dimensions. Before the use of synchrotron radiation a stereo-pair of topographs was two images made with the hkl and $\bar{h}\bar{k}\bar{l}$ reflections (Jenkinson, 1961). They were recorded with a monochromatic beam and needed a rotation of the sample in the goniometer between the exposures. In polychromatic synchrotron radiation topography (Tuomi *et al.*, 1973; Tuomi *et al.*, 1974), any two topographs of a Laue transmission or back-reflection pattern form a stereo-pair (Tuomi *et al.*, 1982), and there is no need to rotate the sample. A stereo-pair of the topographs is used for three-dimensional viewing of a dislocation, *e.g.* with the aid of a stereo viewer, rather than for a quantitative analysis of its direction $\vec{\ell}$. In this work, it is explained how the vector $\vec{\ell}$ is obtained from the topographs recorded on one film under a single exposure.

Another technique suitable for three-dimensional imaging of dislocations and other crystal defects is based on monochromatic beam X-ray topographs (Ludwig *et al.*, 2001; Kawado *et al.*, 2004; Yi *et al.*, 2006). A series of synchrotron X-ray diffraction images are made while rotating the sample in 45° steps and keeping the sample at the same hkl reflection.

Projective properties of an X-ray topography experiment using the continuous spectrum of synchrotron radiation have been studied and used for calculations of a projection of a crystalline direction and of the projected width of a planar object (Miltat & Dudley, 1980). Directions of dislocations have also been calculated by means of vector analysis using the projected directions of the images of the dislocations on the film plane (Yuan & Dudley, 1992).

The goal of this work was to solve a problem: how to determine the direction of a dislocation from a Laue pattern of the diffraction images, *i.e.* of the X-ray topographs, made on a film using synchrotron radiation. An ingenious solution of this inverse problem was successfully found with the aid of descriptive geometry rather than by means of numerical computation and simulation. The data handling leading from the diffraction images to the discovery of the point of intersection is straightforward and an easy task to accomplish. It is also easy to set up and perform in a short time the experiment, in which no beam conditioning like monochromatization or sample alignment or movement are needed. Moreover, the unambiguous determination of the direction of the dislocation in the laboratory frame of reference helps identify and locate the dislocation. It also allows a straightforward calculation of the crystallographic direction of the dislocation as exemplified in this work. Consequently, if the Burgers vector has been determined from the same or similar pattern of topographs, it is possible to tell whether the dislocation is edge, screw or mixed type. All these advantages of the new method are ideal for encouraging and facilitating researchers to apply it to the characterization of defect structures of semiconductors and other monocrystalline materials, semiconductor layer structures and devices in order to improve crystal growth and other fabrication processes.

2. Measurement geometry and analysis

2.1. Geometrical projection

Figure 2(*a*) shows a schematic setup for creating transmission topographs of a single crystal that contains a dislocation $\vec{\ell} = \vec{AB}$, using a Cartesian uvw coordinate system, where the incident X-ray beam is directed downwards along the negative w-axis. A is a point on the front surface and B is a point on the back surface of the crystal. The dislocation $\vec{\ell}$ lies in the plane α defined by points A, B, and origin O. Two parallel rays a and b that correspond to a slice of the incident synchrotron X-ray beam also lie in the plane α. The extension of the dislocation line AB intersects the film plane f at point P, and the v-axis of the uvw coordinate system is chosen to be parallel to $\vec{OP}$. The rays a and b hit the points A and B on the front and back surfaces of the sample, respectively. These rays are diffracted by some (hkl) planes of the crystal lattice. Three unspecified reflections, hkl, are shown in the axonometric representation in Fig. 2(*a*). The n diffraction images A_1B_1, A_2B_2, A_3B_3, ..., A_nB_n of the dislocation $\vec{\ell} = \vec{AB}$, of which the first three are drawn in Fig. 2(*a*), are recorded on the film. The film is a planar foil described by the plane f placed perpendicularly to the incident beam a (and b). Three half-planes of incidence, which are shown in Fig. 2(*a*), are indicated by letters α, β, and γ.

Figure 2(*b*) shows the top view of the topography film f, corresponding to the axonometric picture in cavalier perspective of Fig. 2(*a*). In addition to the diffraction images A_1B_1, A_2B_2, and A_3B_3, Fig. 2(*b*) shows also three more unspecified Bragg reflections A_4B_4, A_5B_5, and A_6B_6 of the dislocation $\vec{\ell}$.

2.2. Dislocation direction theorem and proof

Theorem 1 The extensions of all the dislocation image line segments A_nB_n intersect at a common point P, which lies in

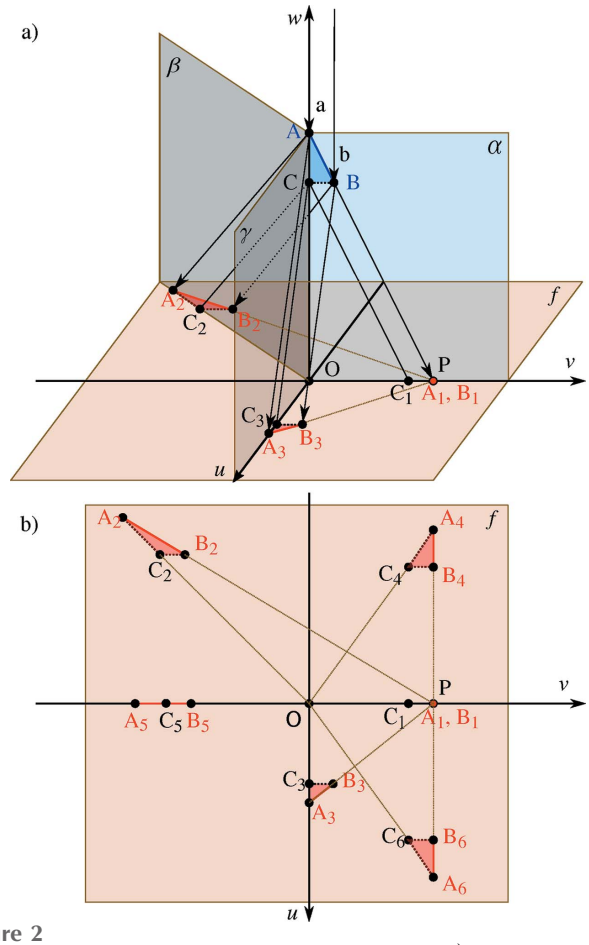

Figure 2
(*a*) Schematic of topography geometry of dislocation $\vec{AB}$, which is divided into two mutually perpendicular components $\vec{AC}$ and $\vec{CB}$. Two rays *a* and *b* of an incident X-ray beam meet the dislocation at its endpoints *A* and *B*. *The v*-axis of the *uvw* coordinate system is chosen to be parallel to $\vec{OP}$. Rays $\vec{AA}_n$ and $\vec{BB}_n$ diffract from dislocation endpoints *A* and *B*, resulting in diffraction images A_1B_1, A_2B_2, and A_3B_3. Similarly projected points C_n of point *C* are also drawn. The zero-length line segment A_1B_1 coinciding with point *P* is a special case, and generally no topograph is guaranteed to be there. (*b*) Top view of film *f* with three additional diffraction images A_4B_4, A_5B_5, and A_6B_6.

the film plane *f* at the extension of the linear dislocation $\vec{\ell} = \vec{AB}$.

The proof of Theorem 1 is based on the geometry of the parallel projection of the X-rays. In order to find the diffraction images of *A* and *B* it is sensible to divide the vector $\vec{\ell} = \vec{AB}$ into two components in the plane α: one component $\vec{AC}$ parallel to the incident beam and the other component $\vec{CB}$ perpendicular to that. Thus, $\vec{AB} = \vec{AC} + \vec{CB}$. It is then found that the image of the component $\vec{CB}$ has an equal length and direction in all topographs on the film,

$$\vec{C_1B_1} = \vec{C_2B_2} = \vec{C_3B_3} = \ldots = \vec{C_nB_n} = \vec{CB} \;\Rightarrow\; C_nB_n = CB. \tag{1}$$

This is a direct consequence of the parallel projection, and the parallelity of the diffracted rays for a particular *hkl* reflection. The image of the other component $\vec{AC}$ has a length and direction that depend on the diffraction angle $2\theta_n = \angle OAA_n = \angle OCC_n$ and the plane of incidence, *i.e.* the plane defined by the incident beam *a* and the diffracted beams $\vec{AA}_n$ and $\vec{CC}_n$.

In Fig. 2(*a*) three diffracted rays that start from point *A* end at points A_1, A_2, and A_3 in the film plane *f*. If there were diffracted rays in the planes of incidence α, β, and γ starting from point *C* and propagating parallel to $\vec{AA}_1$, $\vec{AA}_2$, and $\vec{AA}_3$, they would intersect the film plane at points C_1, C_2, and C_3, and the other reflections *n* produce points A_n and B_n on the film at the dislocation endpoints, which also fix the corresponding points C_n on the film determined by the plane of incidence of the particular diffractions.

It is then clear that all the straight line segments A_1C_1, A_2C_2, and A_3C_3, when extended, intersect at the same point *O* in the center of the film, determined by the incident ray *a*. This follows from the fact that the ray *a* and points *A* and *C* all lie on the *w*-axis. These extended lines are also the plane intersections αf, βf, and γf. This is a direct consequence of the plane of incidence of any reflection: the incident beam *a* and the diffracted beams $\vec{AA}_n$ and $\vec{CC}_n$ are in the same plane of incidence. Considering, for example, the plane of incidence β, it is found that the triangles $\triangle AOA_2$ and $\triangle COC_2$ are similar, because the diffracted rays $\vec{AA}_2$ and $\vec{CC}_2$ are parallel. Because in any reflection *n* there are identically similar triangles, it follows that

$$\triangle AOA_n \simeq \triangle COC_n \;\Rightarrow\; \frac{A_nC_n}{A_nO} = \frac{AC}{AO}. \tag{2}$$

The length of the image A_nC_n on the film is proportional to the distance A_nO of the image from the film center *O*, because A_nC_n/A_nO is constant for every diffraction.

After finding the points A_n, B_n, and C_n, it is possible to define points P_n (for all *n*), which lie at the intersection of the *v*-axis and the extensions of lines A_nB_n, for each *n*. It should be noted that a point P_n does not exist if both points A_n and B_n are on the *v*-axis, which should be treated as a trivial case. Let us now assume that the triangles $\triangle A_nB_nC_n$ exist (*i.e.* no lines A_nB_n lie on the *v*-axis), and consider the triangles $\triangle A_nP_nO$ in the film plane. The triangles $\triangle A_2B_2C_2$ and $\triangle A_2P_2O$ are similar, because $\angle C_2A_2B_2 = \angle OA_2P_2$ and the sides $C_2B_2 \parallel OP_2$. In a general case,

$$\triangle A_nP_nO \simeq \triangle A_nB_nC_n. \tag{3}$$

It follows from equations (3) and (1) that

$$\frac{A_nC_n}{A_nO} = \frac{C_nB_n}{OP_n} = \frac{CB}{OP_n}. \tag{4}$$

Combining equations (2) and (4) leads to

$$\frac{AC}{AO} = \frac{CB}{OP_n} \;\Rightarrow\; OP_n = AO\frac{CB}{AC}, \tag{5}$$

where the last term is constant, and consequently the length of OP_n does not depend on *n*, and all the points P_n coincide. That is, the extensions of the lines A_nB_n intersect at the coincidence point $P_n \equiv P$ for all *n*. This follows from the similarity $\triangle ABC \sim \triangle AP_nO$, which follows directly from equation (5), and consequently shows that the points P_n lie on the extension of the line *AB*.

2.3. Crystallographic direction of dislocation line

Figure 2(*a*) demonstrates that the direction of the dislocation $\vec{\ell} = \vec{AB}$ is parallel to $\vec{AP}$. Consequently, in the laboratory frame of reference, using a Cartesian *xyz* coordinate system, $\vec{AB}$ is known as soon as the point *P* on the film is found using the technique described in Section 2.1. The *z*-axis is chosen to coincide with the *w*-axis of Fig. 2, so that the incident X-rays travel along the negative *z*-axis. The *x*-axis is horizontal and the *y*-axis is vertical. The edges of the rectangular X-ray film are parallel to the laboratory coordinate axes. Thus, the film lies in the *xy* plane of the laboratory frame of reference.

On the film there is a point $P = (P_x, P_y, 0)$, where P_x and P_y are the *x* (horizontal) and *y* (vertical) film coordinates measured from the center of the film at point *O*, through which the incident beam travels. The *uv*-axes are rotated about the *z*-axis by angle $\varepsilon = \arctan(P_y/P_x)$ with respect to the *xy*-axes. The direction of the dislocation in laboratory frame of reference can be given by angles δ_x and δ_y calculated from the equations

$$\delta_y = \arctan\frac{P_y}{L} \quad \text{and} \quad \delta_x = \arctan\frac{P_x}{L} \tag{6}$$

where $L = |\vec{OA}|$ is the film-to-sample distance measured from the top side of the sample to the film surface.

In practice, knowing the angles δ_x and δ_y is often sufficient to exactly determine the dislocation line orientation in the lattice, if the crystal lattice is carefully placed for the topography experiment, *e.g.* so that the principal axes of a cubic crystal are parallel to the *xyz* coordinates. Then, the [*hkl*] direction of the dislocation can be calculated simply using the coordinate (P_x, P_y, L) of the point *P*, and finding the smallest integer triplet *hkl* such that $P_x/h = P_y/k = L/l$. However, if the crystallographic directions of the sample are not readily orientable along the coordinate axes of the laboratory frame of reference, it is advantageous to determine the angle between the X-ray beam and the dislocation line,

$$\delta = \angle OAP = \arctan\frac{|\vec{OP}|}{|\vec{OA}|} = \arctan\frac{\left(P_x^2 + P_y^2\right)^{1/2}}{L}, \tag{7}$$

which can be used in the orientation calculations for the more general case, *e.g.* for non-cubic crystals.

The direction of the dislocation $\vec{AP}$ in the form [*hkl*], relative to the crystallographic directions, can be obtained with the aid of a method based on *stereographic projections* (Cullity, 1956). A stereographic projection consists of poles inside and along the circumference of a *basic circle*. The poles *hkl* are points indicating the normals of the reflecting (*hkl*) planes of the crystal. On the other hand, the position of the point *P* on the film, and its stereographic projection, *i.e.* the pole *P*′, are known by the geometrical analysis to match the direction of the dislocation line $\vec{\ell} = \vec{AB} \parallel \vec{AP}$. The pole *P*′ is then superimposed on the stereographic projection of the known poles of the topography pattern. The direction of the dislocation $\vec{AP}$ is then [*hkl*], where *h*, *k*, *l* are the Miller indices of the pole coincident with the pole *P*′.

3. Two examples

3.1. Large silicon ingot

In this section it is explained how the direction of a linear dislocation is obtained from the synchrotron X-ray transmission pattern of topographs of a silicon single crystal, as per the analysis presented in Section 2 of this work. Figure 3 shows a transmission X-ray diffraction pattern of a (001) silicon sample measured at the TOPO-TOMO measuring station of the KARA (Karlsruhe Research Accelerator) Test Facility and Synchrotron Radiation Source at KIT (Karlsruhe Institute of Technology, Germany). The measurement was set up according to the geometry of Fig. 1. The material was Czochralski-grown silicon, heavily doped with boron to about 10 mΩ cm resistivity. The 4.0 mm-thick sample was cut from the center of a 450 mm-diameter, [001]-oriented crystal, perpendicular to the growth direction. The seed crystal had been lightly doped. In a similar growth process, dislocations due to presumably dopant-induced misfit along the growth axis [001] have been observed (Yonenaga *et al.*, 2002; Taishi *et al.*, 2005).

The tilt angle of the sample was $\Psi = 17°$, and the sample-to-film distance was $L = 61$ mm. There were dislocations to be found very close to the center of the 450 mm-diameter sample, only. This is consistent with the notion that they originate all the way from the neck of the crystal. Six topographs $\bar{4}40$, $\bar{4}00$, 040, $\bar{1}\bar{3}1$, 311, and $4\bar{4}4$ marked on the film are selected for further analysis.

Figure 4 shows these topographs enlarged and put in their proper positions in the diffraction pattern of Fig. 3. There are five parallel dislocation lines visible in each topograph. When these lines are extended they are found to intersect at a point *P* as predicted by the analysis presented in Section 2. In fact,

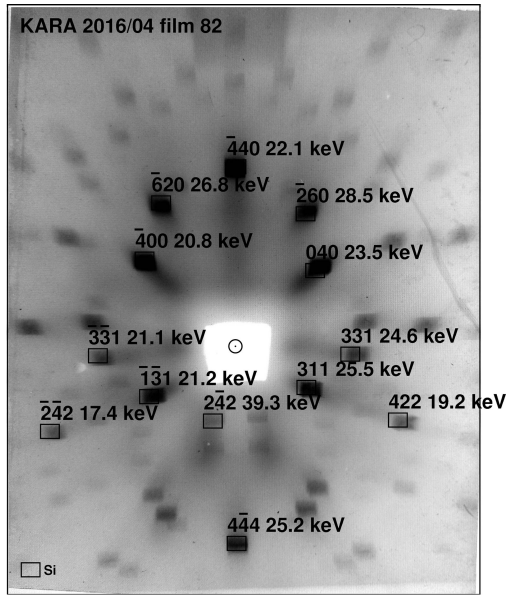

Figure 3
Diffraction pattern of synchrotron transmission topographs of a silicon (001) sample. Simulated diffraction positions with dominant X-ray energies are overlayed on top of the film. The film size is 101 mm × 126 mm.

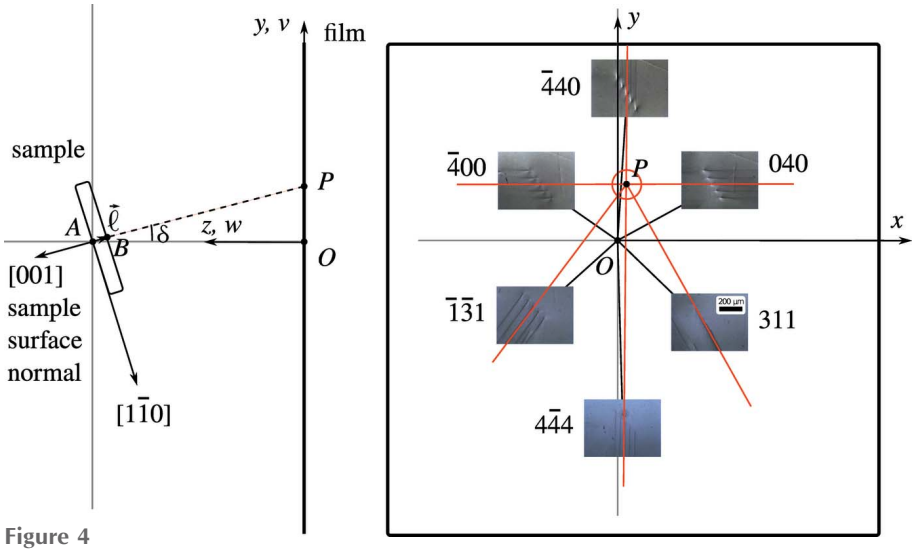

Figure 4
Six enlarged topographs located in their proper positions in the diffraction pattern of a sample cut from a large silicon crystal. Images of dislocation $\vec{\ell}$ are elongated with red lines. Lines intersect at point P determined by angle δ above and right of center O. The thickness of the sample is enlarged for clarity. On the left side, point P and the v-axis are projected to the yz coordinate system.

only two topographs showing unparallel dislocation lines, *e.g.* $\bar{4}00$ and $\bar{4}40$, are needed to determine the point P. However, the redundancy of the topographs in Fig. 4 ensures that no significant measurement errors are present. Figs. 3 and 4 also illustrate the property of the synchrotron topography that one can obtain a number of topographs with a single exposure.

The direction $\vec{\ell}$ of the dislocation is calculated from the distances $|\vec{OP}|$ and $L = |\vec{OA}|$. The angle $\delta = \angle(\vec{AB}, \vec{AO}) = \arctan(|\vec{OP}|/L)$. Using the measured values $L = 61$ mm and $|\vec{OP}| = 18$ mm, from Figs. 3 and 4, it is obtained that $\delta = 16°$. Looking at the experimental setup of Fig. 4 and noticing that $\delta \simeq \Psi = 17°$ it is immediately clear that $\vec{\ell} \parallel [00\bar{1}]$.

The crystallographic direction of the dislocation $\vec{\ell}$ in the form $[hkl]$ can also be obtained by constructing the stereographic projection of the Laue pattern of Fig. 3. The poles of the reflecting planes are plotted by measuring the distances of n diffraction spots, *i.e.* the topographs T_n from the origin O of the film, which is defined as the center of the incident X-ray beam image. They are given by

$$OT_n = L\tan(2\theta_n), \tag{8}$$

where L is again the film-to-sample distance and θ_n is the Bragg angle of each diffraction. The distance of a pole S_n from the center Q of the basic circle of the stereographic projection is given by

$$S_nQ = R\tan(45° - \theta_n/2), \tag{9}$$

where R is the radius of the basic circle, which is twice the radius of the *reference sphere*, *i.e.* $r = R/2$ (Cullity, 1956). The Miller indices of the poles are acquired from the indexed Laue pattern of Fig. 3. By placing the stereographic projection and the film so that the points O and Q coincide, it is apparent that a pole and the corresponding topograph are on the opposite sides of the center and their distances from the center are calculated from equations (8) and (9).

Figure 5 shows the stereographic projection, where the poles are marked with circles, and the respective topographs are indicated as rectangles. In addition, there is the point P of the dislocation direction, corresponding to the dislocation angle $\delta = \arctan(|\vec{OP}|/L) = 16°$. Also, the stereographic projection of the point P is marked as the pole P', the position of which on the stereographic projection is calculated from

$$OP' = R\tan\left(45° - \frac{90° - \delta}{2}\right) = R\tan\left(\frac{\delta}{2}\right), \tag{10}$$

giving approximately 9 mm for values used in Fig. 5. The point P and pole P' are on the same side of the line intersecting the origin O.

In the stereographic projection of Fig. 5 the pole P' (*i.e.* the pole corresponding to the dislocation axis) coincides with the pole [001] within the measurement uncertainty. Consequently, the crystallographic direction of the dislocation $\vec{\ell} = \vec{AB}$ is equal to the Czochralski process growth axis $[00\bar{1}]$, which makes it a rather unusual type of dislocation in silicon (Yonenaga *et al.*, 2002; Taishi *et al.*, 2005).

3.2. Neck of a silicon crystal

As the second example we show the X-ray film (Fig. 6) obtained at the topography measuring station F1 of the former Hamburger Synchrotronstrahlungslabor HASYLAB. The

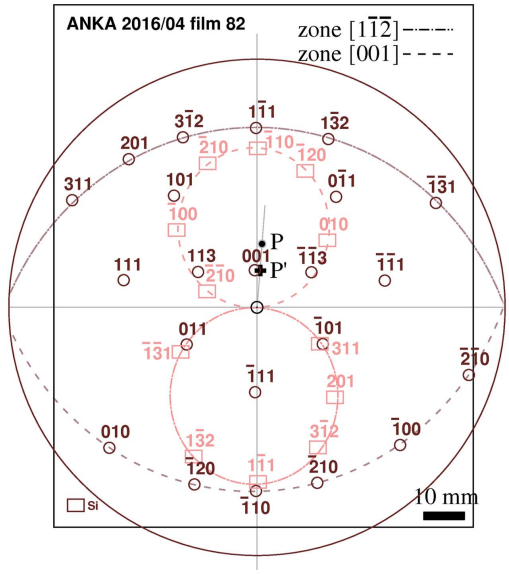

Figure 5
Stereographic projection of poles (circles) corresponding to the topography pattern (rectangles) of a large (001) silicon wafer. Pole P' is a stereographic projection of the dislocation direction point P of Fig. 4. Stereographic circle basic radius $R = 60$ mm. Two zones, $[1\bar{1}\bar{2}]$ and [001], are marked with dashed lines of their own type.

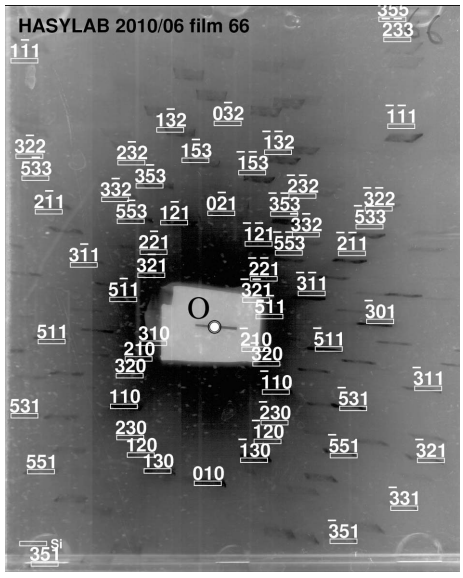

Figure 6
Diffraction pattern of transmission topographs of a silicon (001) wafer from the neck of a silicon crystal. The center of the incident X-ray beam image is defined as the origin O of the film. The film size is 101 mm × 126 mm.

sample was a 2 mm-thick section sliced from a neck of a heavily As doped (001) crystal ingot. The tilt angle was $\Psi = -16°$, and the film-to-sample distance was 62 mm. The calculated diffraction pattern showing the *hkl* Miller indices of selected reflections is overlayed on the film image in Fig. 6.

Figure 7 shows a number of select *hkl* topographs enlarged and located in their proper positions in the diffraction pattern. The five topographs are $2\bar{4}2$, 260, $\bar{2}60$, $\bar{5}11$, and $\bar{5}31$. This illustration is limited to a rather small, 1 mm-wide part of the whole topograph in order to focus the analysis to one particular set of linear dislocations. Furthermore, only one of the nearly parallel dislocations is taken to detailed analysis. The chosen dislocation is visible in all the selected topographs. For example, in the $\bar{5}11$ topograph there are two black lines, of which the right-hand image is the one to be analyzed further.

The dislocation line of each topograph is extended, and they are found to intersect at point P. Comparing Figs. 2 and 7 it can be seen that the point P in Fig. 7 corresponds to the point $A_1 \equiv B_1$ in Fig. 2 although it does not quite lie on the horizontal line as the point $A_1 \equiv B_1$ does, due to a slight rotation of either the film or the sample.

The direction of the dislocation $\vec{\ell}$ is now calculated from the distance $|\vec{OP}|$ and the distance $L = |\vec{OA}|$ between the sample and the film. The angle $\angle(\vec{AB}, \vec{AO}) = \delta = \arctan(|\vec{OP}|/L)$. Using the values $L = 62$ mm and $|\vec{OP}| = 110$ mm, it is found that $\delta = 62°$.

Figure 8 shows the stereographic projection corresponding to the topography pattern in Fig. 6, together with the stereographic projection pole P' of the point P of the dislocation in Fig. 7. The pole P' coincides with the pole $[0\bar{1}1]$. Consequently, the direction of the dislocation $\vec{\ell}$ is parallel to $[01\bar{1}]$.

After having found the direction of $\vec{AP}$, it is feasible to draw a picture similar to Fig. 4, in which the dislocation $\vec{\ell}$ and the crystallographic directions related to the silicon specimen are given. The left part of Figure 7 shows the result. In addition to $\vec{\ell} = \vec{AB}$, the sample normal [001] and the direction [010] are also marked.

In Fig. 7 the angle between the dislocation direction $\vec{\ell}$ and the sample surface normal is 45° (*i.e.* $\vec{\ell} \parallel [01\bar{1}]$). The Burgers vector analysis based on the disappearance of the images of the dislocation with certain Bragg reflections gives $\vec{b} = [\bar{1}10]$. Thus, the analyzed dislocation is a 60° mixed dislocation, *i.e.* $\angle(\vec{\ell}, \vec{b}) = 60°$, a common type in silicon.

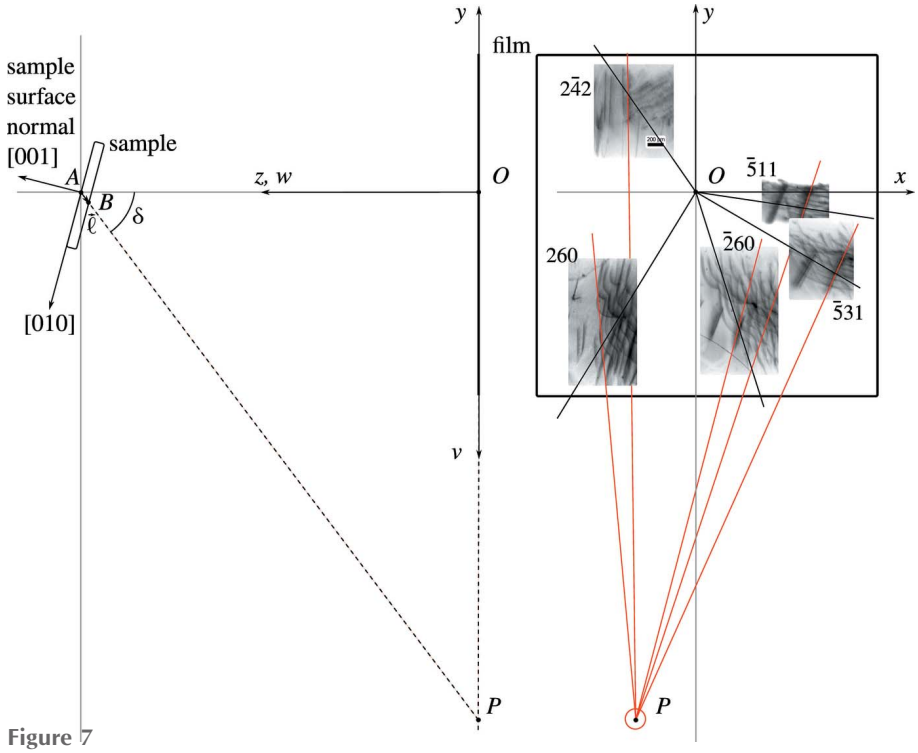

Figure 7
Five enlarged topographs located in their proper positions in a diffraction pattern of a sample cut from neck of a silicon crystal. Images of dislocation $\vec{\ell}$ are continued with red lines, which intersect at point P below and left of center O. The thickness of the sample is enlarged for clarity. On the left side, point P and the v-axis are projected to the yz coordinate system.

4. Conclusions

In this work a new method is described with which the direction of a straight dislocation in a single crystal is determined using descriptive geometry, after an X-ray diffraction topography Laue pattern has been generated on a film by means of synchrotron radiation. There are a number of high-resolution X-ray diffraction images (X-ray topographs) visible on the film. In the

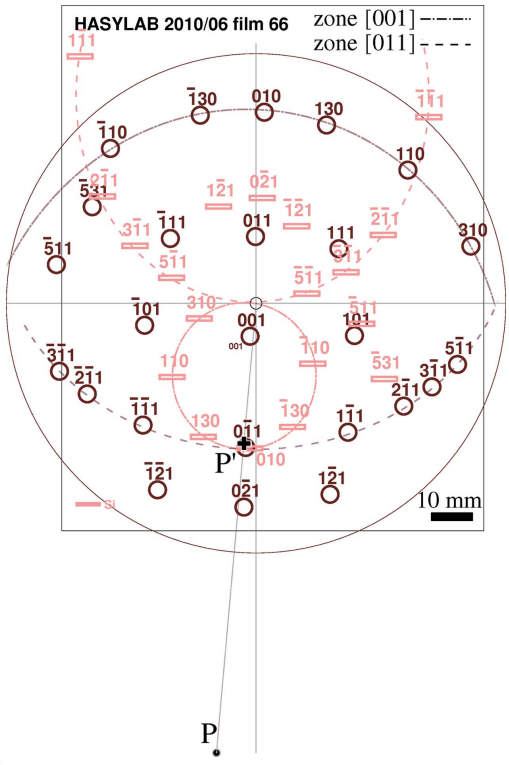

Figure 8
Stereographic projection of poles (circles) corresponding to the topography pattern (rectangles) of Fig. 6. Pole P' is a stereographic projection of the dislocation direction point P of Fig. 7. Stereographic circle basic radius R = 60 mm. Two zones, [001] and [011], are marked with distinctly dashed lines, with matching line types for corresponding on-film zones and stereographic projection zones, which are on opposite sides of the origin.

topographs, a straight dislocation $\vec{\ell}$ is discernible as straight line images.

It is proved with geometric reasoning that the extensions of all the image lines of the dislocation $\vec{\ell}$ intersect at a single point P in the film plane. The location of the point P is found by putting the enlarged topographs in their proper positions at the diffraction pattern, and subsequently elongating the dislocation image lines until they intersect. The direction of the straight dislocation $\vec{\ell} = \vec{AB}$ is equal to the direction of $\vec{AP}$.

The crystallographic direction [*hkl*] of the dislocation $\vec{\ell}$ is calculated by means of the stereographic projection of the poles that correspond to the topography pattern. The *hkl* indices are found by matching the projected dislocation pole P' to one of the known poles of the stereographic projection.

Acknowledgements

The authors would like to thank Professor Dr A. Danilewsky for his invaluable support at the TOPO-TOMO measuring station of the KARA synchrotron radiation facility.

Funding information

The authors acknowledge financial support by the European Community – Research Infrastructure Action under the FP6 'Structuring the European Research Area' Programme (through the Integrated Infrastructure Initiative 'Integrating Activity on Synchrotron and Free Electron Laser Science') under the HASYLAB project DESY-D-II-20060222 EC.

References

Authier, A. (2001). *Dynamical Theory of X-ray Diffraction.* Oxford University Press.
Cullity, B. D. (1956). *Elements of X-ray Diffraction*, 1st ed., *Addison-Wesley Series in Metallurgy and Materials.* Addison-Wesley Publishing Company.
Friedrich, W., Knipping, P. & Laue, M. (1913). *Ann. Phys.* **346**, 971–988.
Jenkinson, A. (1961). *Philips Techn. Rev.* **23**, 82–88.
Kawado, S., Taishi, T., Iida, S., Suzuki, Y., Chikaura, Y. & Kajiwara, K. (2004). *J. Synchrotron Rad.* **11**, 304–308.
Ludwig, W., Cloetens, P., Härtwig, J., Baruchel, J., Hamelin, B. & Bastie, P. (2001). *J. Appl. Cryst.* **34**, 602–607.
Miltat, J. & Dudley, M. (1980). *J. Appl. Cryst.* **13**, 555–562.
Taishi, T., Huang, X., Yonenaga, I. & Hoshikawa, K. (2005). *J. Cryst. Growth*, **275**, e2147–e2153.
Tuomi, T. (2002). *J. Synchrotron Rad.* **9**, 174–178.
Tuomi, T., Kelhä, V., Naukkarinen, K. & Blomberg, M. (1982). *Z. Naturforsch.* **37**, 607–610.
Tuomi, T., Naukkarinen, K., Laurila, E. & Rabe, P. (1973). *Acta Polytechn. Scand.* **100**, 1–8.
Tuomi, T., Naukkarinen, K. & Rabe, P. (1974). *Phys. Status Solidi A*, **25**, 93–106.
Yi, J. M., Chu, Y. S., Argunova, T. S. & Je, J. H. (2006). *J. Appl. Cryst.* **39**, 106–108.
Yonenaga, I., Taishi, T., Huang, X. & Hoshikawa, K. (2002). *Mater. Sci. Eng. B*, **91–92**, 192–195.
Yuan, D. & Dudley, M. (1992). *Mol. Cryst.* **211**, 51–58.